Am J Transl Res 2021;13(5):4007-4025
www.ajtr.org /ISSN:1943-8141/AJTR0128766

Original Article

Exosomes released from mesenchymal stem cells overexpressing microRNA-30e ameliorate heart failure in rats with myocardial infarction

Lianmei Pu[1*], Xiangyun Kong[2*], Hong Li[3], Xue He[1]

[1]Department of Emergency Cardiology, Beijing Anzhen Hospital, Capital Medical University, Beijing 100029, P. R. China; [2]Department of General Medicine, Beijing Luhe Hospital, Capital Medical University, Beijing 101100, P. R. China; [3]Cardiovascular Department, Beijing Anzhen Hospital, Capital Medical University, Beijing 100029, P. R. China. [*]Equal contributors.

Received December 22, 2020; Accepted March 27, 2021; Epub May 15, 2021; Published May 30, 2021

Abstract: Aim: Bone marrow-derived mesenchymal stem cells (BMMSCs) exert cardioprotective effects on myocardial infarction (MI). In this investigation, we elucidated the protective effects of BMMSCs-exosomes (Exo) expressing microRNA-30e (miR-30e) against heart failure (HF) in MI rats. Methods: First, the differentially expressed miRNAs were analyzed using a miRNA-based microarray of MI. Subsequently, we overexpressed miR-30e in rat BMMSCs to isolate exosomes. A rat model with MI was developed and treated with Exo. Next, we examined the cardiac function of the rats, followed by the myocardial tissue extraction. HE, TUNEL and Masson's staining were used to assess the protective effects of exosomes against HF in rats. Subsequently, H9C2 cells exposed to OGD were further co-cultured with Exo. We used bioinformatics to predict the target mRNA of miR-30e and verified the binding relationship. Finally, we tested the expression and role of NF-κB p65/Caspase-9 signaling in myocardial tissues and cells. Results: miR-30e was poorly expressed in myocardial tissues of MI rats. Moreover, treatment of rats with Exo overexpressing miR-30e ameliorated pathological damage, cardiomyocyte apoptosis, and fibrosis in rat myocardial tissues. Furthermore, miR-30e negatively regulated LOX1 expression, which was overexpressed in the MI rats, but further Exo treatment inhibited LOX1 expression. Moreover, Exo overexpressing miR-30e impaired the NF-κB p65/Caspase-9 signaling in myocardial tissues of MI rats. The NF-κB p65/Caspase-9 signaling inhibitor repressed the apoptosis and fibrosis of cardiomyocytes as well. Conclusion: Exosomal miR-30e from rat BMMSCs markedly inhibited LOX1 expression, thereby downregulating the activity of the NF-κB p65/Caspase-9 signaling and ameliorating HF after MI in rats.

Keywords: Myocardial infarction, heart failure, bone marrow-derived mesenchymal stem cells-derived exosome, miRNA-30e, LOX1, NF-κB p65/caspase-9 signaling

Introduction

In China, mortality from acute myocardial infarction (MI) elevated with age irrespective of gender or urban/rural discrepancy, and the most significant increase is seen in patients over 40 years [1]. MI results in cardiomyocyte loss, following ventricular pathological remodeling, damage of cardiac function, and eventually heart failure (HF) [2]. Even though the incidence of acute MI after age-standardization has decreased in a global range, the prevalence of ischemic HF, the most frequent kind of HF, has increased [3]. HF remains a major contributor to hospitalization, poor quality of life, as well as mortality, with a 5-year survival rate of about 50%, but current treatments to prevent or halt progression of HF are limited [4].

Mesenchymal stem cells (MSCs) are classical stem cells with the potency for self-renewal and differentiation in a lot of tissue origins [5]. MSCs are being applied for cardiovascular diseases, including MI, as a regenerative therapy for decades by producing paracrine growth factors which could promote the survivability of neighboring cardiomyocytes [6]. Among them, bone marrow-derived MSCs (BMMSCs), with their characteristics of low immunogenicity and high availability, serve as an ideal cell source in car-

diovascular disease therapy [7]. Within the microenvironment, cells communicate with each other via cell-to-cell contact and extracellular vesicles, which could be categorized into exosomes (Exo, 50-100 nm), microvesicles (100-1,000 nm), as well as apoptotic bodies (larger than 1,000 nm) [8]. The molecular constituents of exosomes include proteins, lipids and nucleic acid cargoes, involving messenger RNA (mRNAs) and noncoding micro-RNAs (miRNAs) [9]. miRNAs are a group of highly conserved non-coding RNAs that are tightly associated with cardiac disorders, involving MI and HF [10]. Moreover, circulating miRNAs are powerful biomarkers for MI as either markers of cardiac ischemic damage or possible regulators of cell/organ function following MI [11]. HF patients have been reported to show a decline in expression of circulating miR-30e-5p relative to matched patients without HF [12]. Interestingly, our prediction using miRNA expression microarray GSE95855 from the GEO public database (https://www.ncbi.nlm.nih.gov/geo/) revealed that miR-30e was the most significantly downregulated miRNA in myocardial tissues between MI and sham-operated rats. Therefore, we determined miR-30e as our study subject. We hypothesized that BMMSCs secrete miR-30e-enriched Exo to protect myocardial tissues from injury. In this work, the roles of miR-30e in Exo-modulated cardioprotective effects were investigated in Sprague-Dawley (SD) rats induced with left anterior descending (LAD) artery ligation and in H9C2 cells under the exposure oxygen-glucose deprivation (OGD).

Materials and methods

Animals

Animal experiments were permitted by the Ethics Committee of the Beijing Anzhen Hospital, Capital Medical University as per the Animal Welfare Act and PHS Policy on Humane Care and Use of Laboratory Animals. A total of 36 male SD rats (180-200 g) were purchased from Vital River (Beijing, China) and housed in a room on a 12/12 h light/dark cycle with ad libitum access to chow and drinking water.

Extraction, identification and treatment of rat BMMSCs

BMMSCs were separated as previously described [13]. Briefly, BMs were acquired from tibia and femur of healthy rats by flushing with DMEM (D5648, Sigma, Saint Louis, MO, USA) under sterile conditions. The suspensions were harvested by centrifugation and treated with erythrocyte lysis buffer (R1010, Solarbio, Beijing, China) to deplete the erythrocytes. The cells were resuspended and incubated in DMEM plus FBS at 37°C with 5% CO_2.

To identify BMMSCs, the immunophenotypes of isolated BMMSCs were evaluated by flow cytometric analysis. BMMSCs were negative for CD34 and CD45, whereas positive for CD29 and CD90. Osteogenic and adipogenic differentiation was examined on BMMSCs by a 21-d incubation in osteogenic and adipogenic differentiation medium. The cells were then fixed and stained with Oil Red O (G1262, Solarbio) or Alizarin Red (G1450, Solarbio).

MiR-30e-5p was delivered into BMMSC by a lentiviral vector (LV)-modulated approach. BMMSCs (1×10^5) were infected with LV-miR-30e-5p or empty vector with a MOI of 20 and then left overnight at 37°C with 5% CO_2. Afterwards, the medium containing LV was refreshed with DMEM plus 10% FBS for another 24-h incubation.

Extraction and identification of Exo released from BMMSCs

Ultracentrifugation was used to separate and extract Exo. When BMMSCs approximately reached an 80% confluence, the supernatant was removed and supplemented with serum-free medium for a 48-h incubation. The samples were centrifuged at 300 g for 5 min and at 2,000 g for 20 min. The conditioned medium was filtered through a 0.22 μm filter and centrifuged twice at 100,000 g for 90 min. The obtained precipitate was resuspended in PBS and preserved at -80°C.

To verify the Exo, the morphology was observed under a TEM (JEM-1400, JEOL, Japan). Next, the size distribution and particle concentration of Exo were assessed using Nanoparticle tracking analysis (NTA). TSG101, Alix, CD81 expression was assessed by western blot.

H9C2 cells were treated with PKH67-labelled (Sigma-Aldrich, Merck KGaA, Darmstadt, Germany) Exo (20 μg/mL) in DMEM plus 10% FBS. For animal treatment, labelled Exo (20 μg/mL) was injected into the tail vein of rats. At 7 d

post-injection or 48 h post-culture, myocardial tissues or H9C2 cells were fixed in 4% paraformaldehyde and loaded onto an Olympus BX41 microscope equipped with a charge-coupled device (MagnaFire, Olympus Optical Co., Ltd., Tokyo, Japan).

Bioinformatics analysis

First, we downloaded a miRNA expression microarray GSE95855, which contained myocardial tissue samples from three MI rats and three sham-operated rats, respectively, from the GEO database. Differential screening was then performed by setting Log FoldChange > 2 (for miRNAs) or 1 (for mRNAs) and adj *p* value < 0.05 as thresholds. Subsequently, target mRNAs for miR-30e were predicted via StarBase and TargetScan websites, and intersected with genes upregulated in the GSE35088 dataset. The Calculate and draw custom Venn diagrams website was then utilized to plot a Venn map.

Animal model and treatment

Coronary artery ligation was applied for MI establishment. Briefly, rats (180-200 g) were subjected to the LAD artery ligation or the sham operation after anesthesia with sodium pentobarbital at 50 mg/kg (i.p.). A left intercostal thoracotomy was conducted to expose the heart, and the left coronary artery was ligated with a single nylon suture. Afterwards, the heart was then repositioned to the chest. Except for no ligation for the left anterior descending artery, sham-operated rats had the same procedure.

To determine the role of BMMSC-derived Exo in MI-induced HF, we injected BMMSC-derived Exo into rats via the tail vein for three consecutive days beginning at 7 days after MI surgery. Four weeks after injection, rats were euthanized with pentobarbital sodium at 100 mg/kg (i.p.).

Assessment of heart functions

Anesthesia was induced with 2.0% isoflurane. Scans were conducted with the help of an ultrasound system (VisualSonics, Toronto, Canada) equipped with a 21-MHz probe. The average of three consecutive cardiac cycles data was taken. Ejection fraction (EF) and fractional shortening (FS) of the left ventricle were assessed. The left ventricular end-systolic diameter (LVESD), left ventricular end-diastolic diameter (LVEDD), left ventricular volumes in systole (LVVs), and left ventricular volumes in diastole (LVVd) were then assessed.

The left ventricle of rats was inserted with a conductance micromanometer catheter (1.4F, Millar Instruments, Houston, TX, USA) via the left carotid artery. A PowerLab data acquisition system (AD Instruments, Sydney, Australia) was used to measure the $+dp/dt_{max}$ and $-dp/dt_{max}$, left ventricular systolic pressure (LVSP), and left ventricular end-diastolic pressure (LVEDP).

HE staining

The left ventricle was placed in 10% formaldehyde solution, dehydrated in an ethanol gradient, paraffin-embedded, and cut into 4-μm sections. After removal of paraffin, the sections were stained with hematoxylin-eosin, mounted, and viewed under an optical microscope (Leica Microsystems, Wetzlar, Germany). After examination under screening power (40 ×), at least 20 low power fields (100 ×) of each slide were taken to search for necrosis, hemorrhage, inflammation, as well as myocardial degeneration. Percent of these changes in each field was roughly estimated with naked eyes, and the final results were the average of the 20 fields. High power field (400 ×) examination was conducted as well for confirmation. The abnormality was scored as 0 (0%), 1 (1-25%), 2 (26-50%), 3 (51-75%), and 4 (76-100%) as per the percentage of histopathological changes.

Masson's staining

The myocardial tissues were fixed with 10% formaldehyde overnight, decalcified, dehydrated, permeabilized using xylene, paraffin-embedded, and cut into 5 μm sections. Cell nuclei were stained for 5 min using Wiegert's hematoxylin solution (Sigma-Aldrich, St. Louis, MI, USA). After being stained with 0.7% Masson-Ponceau-acid fuchsin (Sigma-Aldrich) for 10 min, the samples were washed in 2% glacial acetic acid, fractionated in phosphomolybdic acid for 4 min and stained with 2% aniline blue solution (Sigma-Aldrich). After a series of treatments using ethanol gradient, xylene and neutral resin, images were viewed by an optical microscopy.

Tripheny tetrazolium chloride (TTC) staining

Evans-Blue staining (2.0% solution in 1 mL) was injected into the coronary circulation via a

carotid catheter. The hearts were promptly excised and frozen at -20°C for 0.5 h, then sequentially cut into 1-mm sections and incubated in 1.0% TTC-contained PBS (pH = 7.4) at 37°C for 15 min. Image-Pro Plus software was utilized to assess the volume of normal (non-at-risk, ANAR), ischemic (at-risk, AAR), and infarcted (INF) regions, and the results were considered as INF/AAR × 100%.

TUNEL staining

For TUNEL staining, the sections were first dried at ambient temperature for 10 min and detached with 5 μg/mL proteinase K (Roche Diagnostics, Indianapolis, IN, USA) at 37°C for 20 min. The sections were then subjected to TUNEL staining (In Situ Death Detection Kit, 1684795, Roche) as per the manufacturer's protocol. The nuclei were then stained with Hoechst. The images were taken and analyzed by two researchers who had no knowledge of the study using the Cellsens imaging system.

Immunohistochemistry

For immunohistochemical staining, the HE staining procedure described above was followed, and the tissues were sealed with goat serum for 0.5 h at ambient temperature and treated overnight at 4°C with primary antibodies to alpha-smooth muscle actin (α-SMA), LOX1, phos-NF-κB p65, and caspase-9. The tissues were probed with HRP-labeled secondary antibodies in the dark for 1 h, followed by diaminobenzidine treatment and hematoxylin counter-staining. The sections were viewed under an optical microscope, and the images were captured using Image J software (WS Rasband, NIH, http://imagej.nih.gov/ij/).

ELISA

Serum CK-MB and cTnI levels are specific indicators of the extent of myocardial damage. After MI surgery, rat arterial blood was collected, and then serum CK-MB (#H197) and cTnI (#E019-1-1) levels were assessed using ELISA kits (JianCheng, Jiangsu, China).

Cell culture and treatment

Rat cardiomyocyte H9C2 were from Shanghai Institute of Cell Biology (Shanghai, China). H9C2 cells were grown in DMEM containing 10% FBS (both from Gibco, Carlsbad, CA, USA) at 37°C and 5% CO_2. The constructed LOX1-overexpressing plasmid and its empty plasmid were transfected into the cells in good growth condition using Lipofectamine 2000. Briefly, 5 μg plasmid was mixed with 5 μL Lipo 2000 in a centrifuge tube. After 20 min of resting, the plasmid-lipo mixture was added to a six-well plate for transfection. After 12 h of transfection, the fresh medium was replaced for another 24 h incubation. After that, the cells were harvested for following experiments.

The glucose-free medium was exposed to hypoxic conditions (95% N_2 and 5% CO_2) for 5 min. Exo-treated cardiomyocytes were grown in hypoxia/hypoglycemia medium in a Napco 8000 w hypoxia incubator (1% O_2, 5% CO_2, 94% N_2) for 9 h. The incubation continued for another 3 h in medium with normal glucose concentrations under conventional conditions. Alternatively, following OGD treatment, H9C2 cells were incubated with 100 μM NF-κB specific inhibitor FW1256 (HY-121955, MedChemExpress, Monmouth Junction, NJ, USA) or dimethylsulfoxide (DMSO) and collected after 24 h for subsequent experiments.

EdU staining

The activity of H9C2 cells was evaluated using BeyoClick™ EdU cell proliferation kit and Alexa Fluor 555 (Beyotime, Shanghai, China). In detail, cells were plated in 6-well plates containing 10 μM EdU reagent and incubated at 37°C for 2 h. The cells were then fixed with 500 μL 4% paraformaldehyde, cultured with permeable solution, and incubated with 500 mL Click reaction solution for 0.5 h at ambient temperature in darkness, followed by an incubation with 4',6-diamidino-2-phenylindole for 15 min. EdU-positive cells were viewed under an inverted fluorescence microscope (Olympus) and analyzed by Image J software.

Flow cytometry

A flow cytometer (Nanjing KeyGen Biotech Co., Ltd., Nanjing, Jiangsu, China) was applied. Cells were cultured overnight with 1×10^5 cells/well in a 6-well culture plate and incubated with Exo or PBS prior to hypoxia treatment. Afterwards, cells were treated using the Annexin V-FITC/PI apoptosis kit (KeyGen Biotech) and analyzed with the help of Flowjo software (version 10.0, TreeStar, Ashland, OR, USA).

Table 1. Primer list

Symbol	Species	Forward (5'-3')	Reverse (5'-3')
miR-30e	Rattus norvegicus	TGTAAACATCCTTGACTGG	GAACATGTCTGCGTATCTC
U6	Rattus norvegicus	CTCTCGCTTCGGCAGCACA	ACGCTTCACGAATTTGCGT
LOX1	Rattus norvegicus	GTCATCCTCTGCCTGGTGTTG	TGCCTTCTGCTGGGCTAACATC
GAPDH	Rattus norvegicus	GCAAGGATGCTGGCGTAATG	TACGCGTAGGGGTTTGACAC
α-SMA	Rattus norvegicus	CTATGCCTCTGGACGCACAACT	CAGATCCAGACGCATGATGGCA
FN-1	Rattus norvegicus	CCCTATCTCTGATACCGTTGTCC	TGCCGCAACTACTGTGATTCGG

Note: miR-30e, microRNA-30e; LOX1, lectin-like oxidized low-density lipoprotein receptor-1; GAPDH, glyceraldehyde 3-phosphate dehydrogenase; α-SMA, alpha-smooth muscle actin; FN-1, fibronectin 1.

Lactate dehydrogenase (LDH) cytotoxicity test

After being seeded in 96-well plates at 2×10^4 cells/well, the cells were treated as described previously. A total of 10 μL cell culture medium was aspirated at the indicated time points, diluted at 1:10 with LDH storage buffer containing 200 μM Tris-HCl (pH = 7.3), 10% glycerol, and 1% bovine serum albumin (BSA), and stored at -20°C. After thawing, samples were analyzed using the LDH-Glo cytotoxicity assay (Promega Corporation, Madison, WI, USA).

Immunofluorescence staining

Rat cardiomyocytes were incubated and then exposed to medium containing Exo or PBS for 48 h. After that, the slides were fixed in 4% paraformaldehyde and permeabilized with HEPES-250 Triton X100 buffer (Sigma). Staining was performed using rabbit anti-rat antibodies to α-SMA (1:200; ab7817, Abcam) and FN-1 (1:200; ab2413, Abcam) at 4°C for one night. Then, FITC-coupled secondary antibodies (ZSGB-Bio, Beijing, China) were added for a 1 h incubation at 37°C. Fluorescence was assessed in the dark by a microscope (TE2000, Nikon Instruments Inc., Melville, NY, USA).

RT-qPCR

A 7900HT real-time PCR detection system (Thermo Fisher Scientific Inc., Waltham, MA, USA) was utilized for RT-qPCR. Briefly, cellular and exosomal total RNA was isolated using Trizol reagent (Life Technologies, Carlsbad, CA, USA). To quantify mRNA expression, first-strand cDNA was produced with random primers using a PrimeScript™ RT kit (Takara Holdings Inc., Kyoto, Japan) with a gDNA eraser. Stem-loop RT-qPCR was conducted using FastStart Essential DNA Green Master (Roche). To quantify miR-30e expression, cDNA was produced using the miRNA first-strand cDNA synthesis kit (by stem-loop method) (NanJing Vazyme Biotech Co., Ltd., Nanjing, China). Real-time PCR was then implemented using AceQ qPCR SYBR Green Master Mix (Vazyme Biotech). The expression was normalized to U6 (for miR-30e) or glyceraldehyde 3-phosphate dehydrogenase (GAPDH) (for mRNA) using the $2^{-\Delta\Delta Ct}$ method. The primer sequences are shown in **Table 1**.

Western blot assays

Cells were ice-bathed for 30 min with lysis buffer, and the total cellular protein concentration was assessed using the BCA assay protein assay kit. Total protein (30 μg) was separated by SDS-polyacrylamide gel electrophoresis (Invitrogen Inc., Carlsbad, CA, USA). After protein transferring, the PVDE membranes (Roche) were sealed with 5% BSA in Tris-buffered saline-Tween (0.1%) and incubated against the antibodies. Antibodies included the primary antibodies against NF-κB p65 (8242, Cell Signaling Technology), phos-p65 (3036, Cell Signaling Technology), Caspase-9 (40675, Signalway Antibody, College Park, MA, USA), LOX1 (PA5-95750, Thermo Fisher), GAPDH (5174, Cell Signaling Technology), TSG101 (14497, ProteinTech Group, Chicago, IL, USA), CD81 (66866, Proteintech) and Alix (ab117600, Abcam), and HRP-conjugated secondary antibody (Santa Cruz Biotechnology Inc., Santa Cruz, CA, USA). Blots were visualized using enhanced ECL reagents and analyzed using a gel recording system (Bio-Rad Gel Doc 1000 and Multi-Analyst version 1.1).

Luciferase activity assay

The LOX1 3'untranslated region (3'UTR) cDNA fragment containing the miR-30e binding site

was amplified by PCR. The amplified product was cloned into a PGL3 vector (Promega) downstream of the reporter gene with a translation termination codon. Mutants of LOX1 were created with the help of the Takara MutanBEST kits (Takara). HEK-293T cells in 24-well plates were transfected with luciferase reporter constructs at 200 ng/well and miR-30e mimic or mimic control at 400 ng/well with the help of Lipofectamine 2000. Internal control was the SV-Renilla luciferase plasmid (5 ng/well). Twenty-four h after transfection, cells were collected, and the luciferase activity was assessed using the Dual-Luciferase Reporter Assay Kit (Promega). Renilla luciferase activity served as an internal control, and the ratio of firefly luciferase luminescence relative to control was measured.

RNA immunoprecipitation (RIP)

H9C2 cells from each group were collected and centrifuged at 1500 rpm for 5 min. Then, a volume of RIP lysis buffer was mixed thoroughly with the cells. The beads were resuspended. After that, 5 μg Ago2 antibody (ab32381, 1:50; Abcam) was supplemented, while the cells were probed with IgG antibody for 30 min at ambient temperature as a negative control. The cells were rinsed two times with 500 μL RIP wash buffer to remove the supernatant. The cells were supplemented with 500 μL RIP wash buffer for shaking and kept on ice for later use. After the removal of the supernatant from the magnetic bead tubes, 900 μL RIP buffer was added to each tube. The cell lysates were centrifuged at 14,000 rpm at 4°C for 10 min. Then, 100 μL supernatant was added to the bead-antibody complex so that the final volume was 1 mL for an overnight incubation at 4°C. After instantaneous centrifugation to remove the supernatant, 500 μL RIP wash buffer was supplemented and shaken to remove the supernatant. Following the addition of 150 μL proteinase K buffer, the bead-antibody complex was allowed to resuspend at 55°C for 0.5 h. The RNA was then extracted for RT-qPCR.

Statistics

The values were showed as the mean ± SD. Comparisons between two observations were evaluated by unpaired *t* test. One-way or two-way ANOVA and the Tukey's post hoc analysis were conducted when multiple comparisons were made using GraphPad Prism 8 software (GraphPad, San Diego, CA, USA). Statistical significance was considered at a value of $P < 0.05$.

Results

miR-30e is poorly expressed in the myocardial tissues of MI rats

We first downloaded the miRNA expression microarray GSE95855 for rats with MI from the GEO database, which contained myocardial tissue samples from three MI rat and three sham-operated rats. The microarray was then screened for differences by setting Log FoldChange > 1 and Adj *p* value < 0.05 as screening thresholds. A total of 26 differentially expressed miRNAs are shown in **Figure 1A**, **1B**. It was found that miR-30e was the most remarkably downregulated one in MI. To verify the role of miR-30e, we firstly induced a rat model of MI by LAD and found that EF and FS were notably decreased, while LVEDD, LVESD, LVVs and LVVd were significantly enhanced in MI rats (**Figure 1C**). Subsequently, the levels of the myocardial injury-related proteins CK-MB and cTnI in the serum of rats with MI were significantly increased by ELISA (**Figure 1D**). Moreover, TTC staining revealed significantly larger infarct size in myocardial tissues in rats after LAD surgery than that in sham-operated rats (**Figure 1E**). The above results indicated the successful development of a rat model of MI with HF. Subsequently, the RT-qPCR assay displayed that miR-30e was notably diminished in the myocardial tissues of MI rats (**Figure 1F**). So, we wondered if some kind of "medium" could be used to deliver exogenous miR-30e to MI rats, which could be applied to treat HF in MI.

Rat BMMSC-derived Exo are successfully isolated

We first used flow cytometry to identify cells that were isolated from rat tibia and femur, and we observed that the cells were negative for CD34 and CD45 and strongly positive for CD29 and CD90 (**Figure 2A**). After treating the cells with osteogenic and adipogenic differentiation media, respectively, the extracted cells showed potential for adipogenic and osteogenic differentiation, as evidenced by alizarin red staining as well as oil red O staining (**Figure 2B**). The above results meet the definition of BMMSCs. Subsequently, we extracted Exo from the condi-

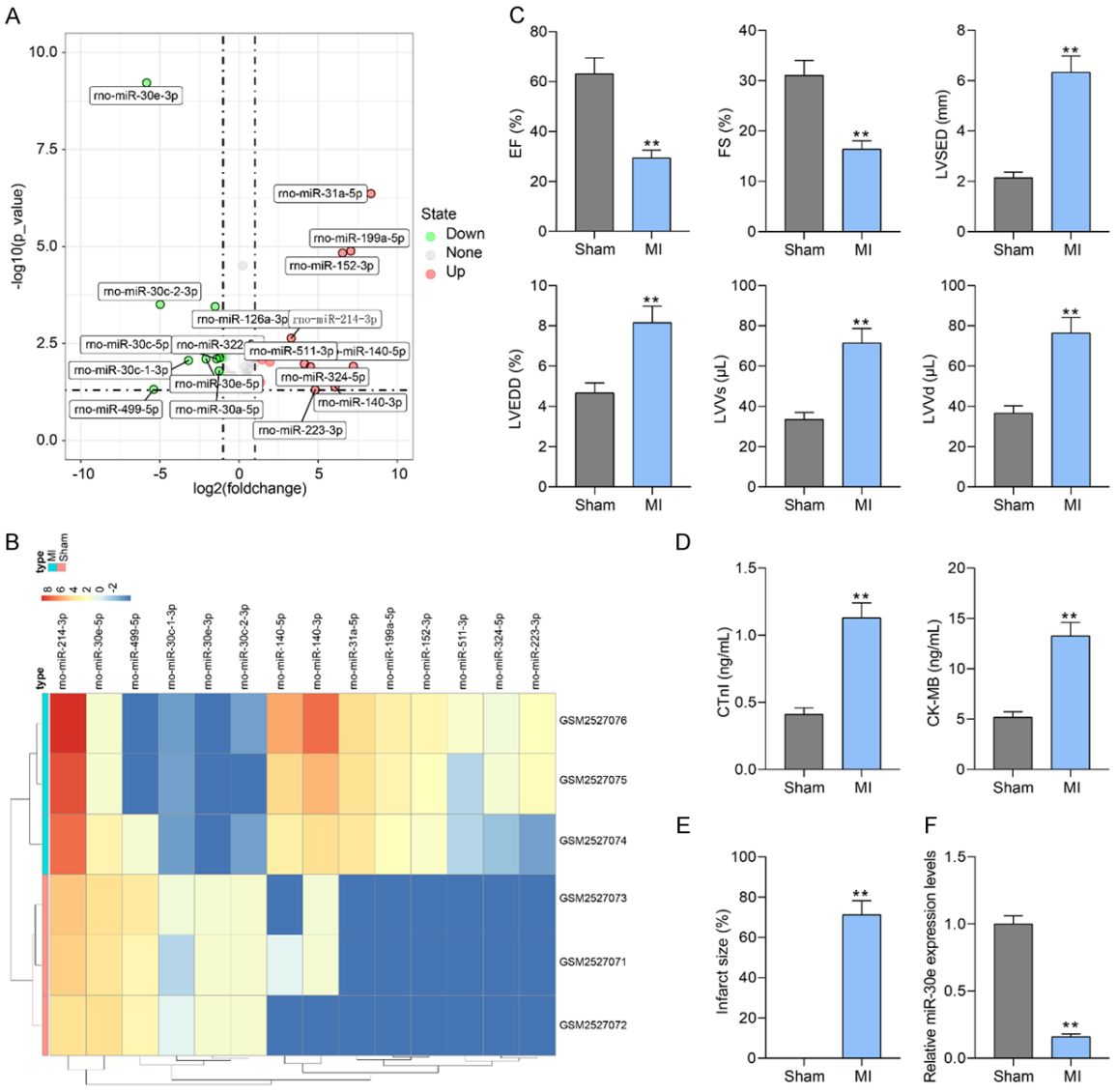

Figure 1. miR-30e is depleted in the myocardial tissues of MI rats. (A) The volcano map for differentially expression miRNAs in GSE95855 (n = 3); (B) The heatmap for differentially expression miRNAs in GSE95855 (n = 3); (C) EF, FS, LVEDD, LVESD, LVVs and LVVd values in rats; (D) ELISA for the detection of myocardial injury-related proteins CK-MB and CTnI in the serum of rats; (E) Staining and statistical analysis of infarct size in rat myocardial tissues after LAD surgery; (F) Expression of miR-30e in rat myocardial tissues by RT-qPCR. For (C-F), each group contained 6 rats (unpaired *t* test). Error bars represent the mean ± SD. $^{**}P < 0.01$ *vs* sham-operated rats.

tioned medium of BMMSCs by gradient centrifugation. Firstly, TEM disclosed that the extracted "extracellular vesicles" were oval-shaped or barrel-shaped (**Figure 2C**). NTA revealed that the size distribution was in the range of 44.19-107.22 nm (**Figure 2D**). Moreover, they were positive for the exosomal marker proteins CD9, CD63, Alix, and CD81, as displayed by western blot (**Figure 2E**). To use Exo for delivery of miR-30e for the treatment of HF, we overexpressed miR-30e in BMMSCs and confirmed the successful overexpression using RT-qPCR (**Figure 2F**). The cellular phenotype of BMMSCs analyzed by flow cytometry did not change (**Figure 2G**), indicating that overexpression of miR-30e did not affect the cellular properties of BMMSCs. Subsequent extraction of Exo using gradient centrifugation and detection of miR-30e expression in Exo using RT-qPCR revealed that Exo derived from BMMSCs overexpressing

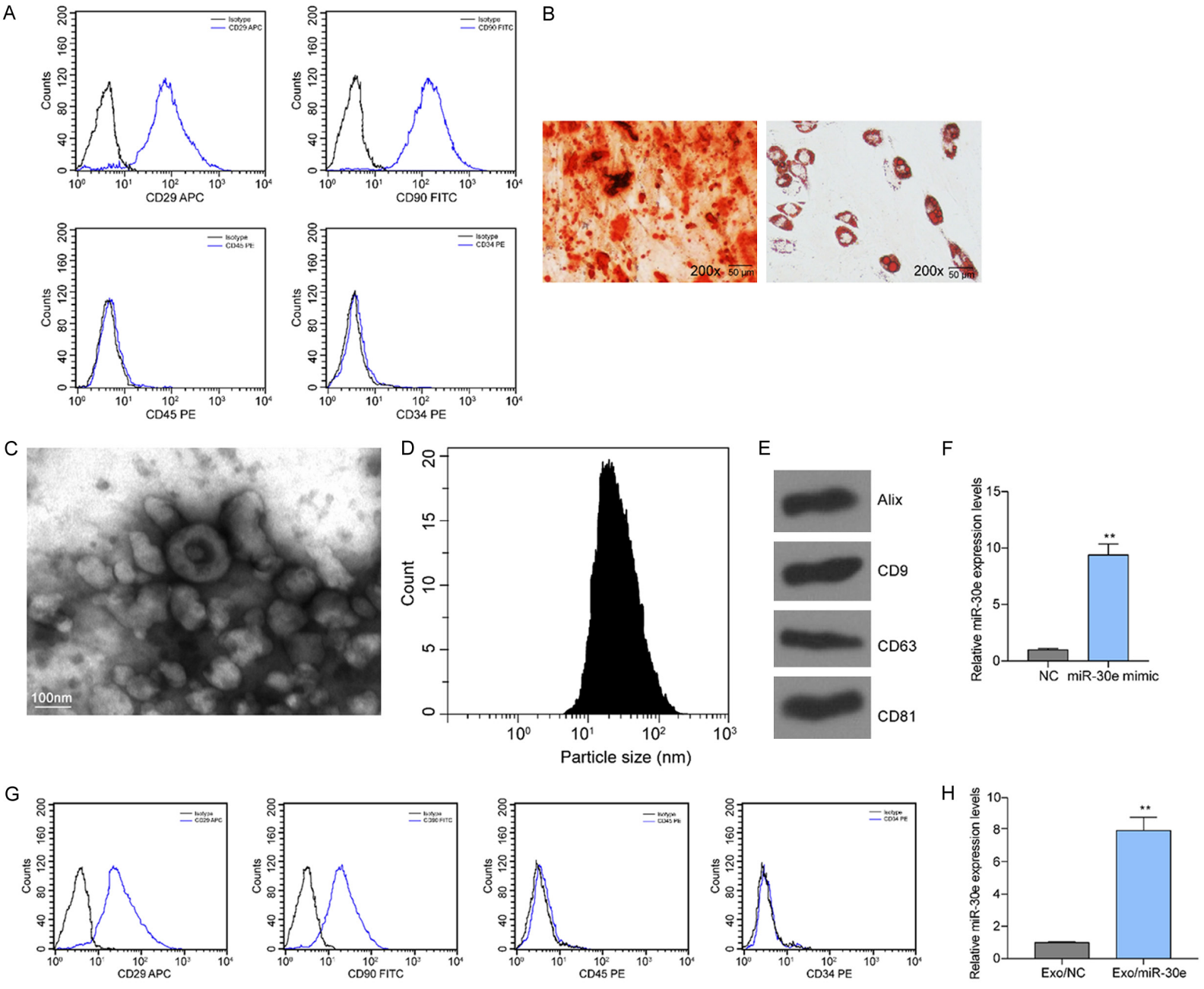
A
Isotype
CD29 APC
Counts
CD29 APC
Isotype
CD90 FITC
CD90 FITC
Isotype
CD45 PE
CD45 PE
Isotype
CD34 PE
CD34 PE
B
200x 50 μm
200x 50 μm
C
100nm
D
Count
Particle size (nm)
E
Alix
CD9
CD63
CD81
F
Relative miR-30e expression levels
NC
miR-30e mimic
G
CD29 APC
CD90 FITC
CD45 PE
CD34 PE
H
Relative miR-30e expression levels
Exo/NC
Exo/miR-30e

Figure 2. Characterization of Exo derived from BMMSCs. (A) Flow cytometric identification of hematopoietic markers CD34 and CD45, and MSCs-specific markers including CD29 and CD90 in extracted cells; (B) Identification of adipogenic and osteogenic differentiation of the extracted cells; (C) TEM analysis of the shape and size of the extracted Exo; (D) Particle size distribution by NTA; (E) Western blot detection of the exosomal marker proteins CD9, CD63, Alix, and CD81 expression; (F) The miR-30e expression in the BMMSCs transfected with miR-30e mimic or NC examined by RT-qPCR; (G) Flow cytometric identification of hematopoietic markers CD34 and CD45, and MSCs-specific markers including CD29 and CD90 in BMMSCs transfected with miR-30e mimic or NC; (H) The miR-30e expression in Exo derived from BMMSCs transfected with miR-30e mimic or NC examined by RT-qPCR. Error bars represent the mean ± SD. The results of the experiment were tested in three separate trials. For (F and H), unpaired *t* test. $^{**}P < 0.01$ *vs* BMMSCs transfected with NC or Exo derived from those cells.

miR-30e (Exo/miR-30e) exhibited increased expression of miR-30e relative to Exo derived from BMMSCs transfected with negative control (Exo/NC) (**Figure 2H**).

Exo/miR-30e alleviates HF in MI rats

To clarify the therapeutic effect of BMMSC-derived Exo on HF of rats with MI, we injected PBS, Exo, Exo/NC, and Exo/miR-30e into rats at a dose of 20 μg/mL through the tail vein. The distribution of PKH67 in rat myocardial tissues was observed under a fluorescence microscope 7 days later, and the results showed that rat myocardial tissues took up BMMSC-derived Exo (**Figure 3A**). Subsequently, we tested the cardiac function of rats and found that after Exo treatment, LVEF and LVFS increased, while LVEDD, LVESD, LVVs, and LVVd significantly decreased. Further increases in Exo-carrying miR-30e had a further improvement in cardiac function (**Figure 3B**). Furthermore, Exo treatment notably downregulated the serum levels of CK-MB and cTnI in rats, while Exo/miR-30e treatment further ameliorated cardiac injury in rats (**Figure 3C**). TTC staining revealed that Exo treatment significantly reduced the infarct area in rats, and after increasing Exo-carrying miR-30e, the infarct area had a further decline (**Figure 3D**). HE staining showed that the pathological damage scores of myocardial tissues were lowered after Exo treatment, and the therapeutic effect of Exo in HF rats was further enhanced by increasing the miR-30e expression (**Figure 3E**). The above findings indicate that overexpression of miR-30e contained by BMMSC-derived Exo can significantly ameliorate HF in rats with MI.

Exo/miR-30e inhibits MI-induced myocardial injury

To clarify the mechanism underlying the therapeutic effect of BMMSC-derived Exo on HF, we first used Masson's staining to assess the area of collagen deposition in the myocardial tissues of rats, and we found that Exo treatment significantly reduced fibrotic areas in the myocardial tissues (**Figure 4A**). Similarly, the staining intensity of the fibrosis-related factor α-SMA in myocardial tissues by immunohistochemical staining revealed that Exo treatment significantly reduced α-SMA level (**Figure 4B**). And then, we used TUNEL staining to find that the apoptosis in rat myocardial tissues was significantly reduced after Exo treatment (**Figure 4C**). The angiogenesis-related factor CD31 and anti-inflammatory factor CD206 in rat myocardial tissues examined by immunohistochemistry illustrated that angiogenesis was significantly elevated (**Figure 4D**), while the inflammatory response was alleviated (**Figure 4E**) in MI rats after Exo treatment. Furthermore, we found that increasing Exo-carrying miR-30e further reduced the level of fibrosis, the proportion of apoptotic cells, and promoted myocardial regeneration and suppressed MI-induced inflammation in the myocardial tissues of rats with MI (**Figure 4A-E**).

Exo/miR-30e inhibits apoptosis in OGD-treated cardiomyocytes

To validate the therapeutic effect of BMMSC-derived Exo on MI at the cellular level, we treated rat cardiomyocytes H9C2 with OGD and subsequently co-cultured with Exo. The cellular activity of H9C2 cells was inhibited after OGD treatment, but restored after treatment with Exo. Further increase of miR-30e carried in Exo greatly promoted cellular activity (**Figure 5A**). Moreover, flow cytometry detection revealed that OGD treatment significantly enhanced the proportion of apoptosis in H9C2 cells, but Exo treatment remarkably downregulated the number of apoptotic cells. In addition, the effect of Exo/miR-30e on the inhibition of OGD-induced apoptosis was more pronounced (**Figure 5B**). Subsequently, we used an LDH cytotoxicity kit to detect cytotoxicity caused by OGD, and the obtained results were consistent with that of

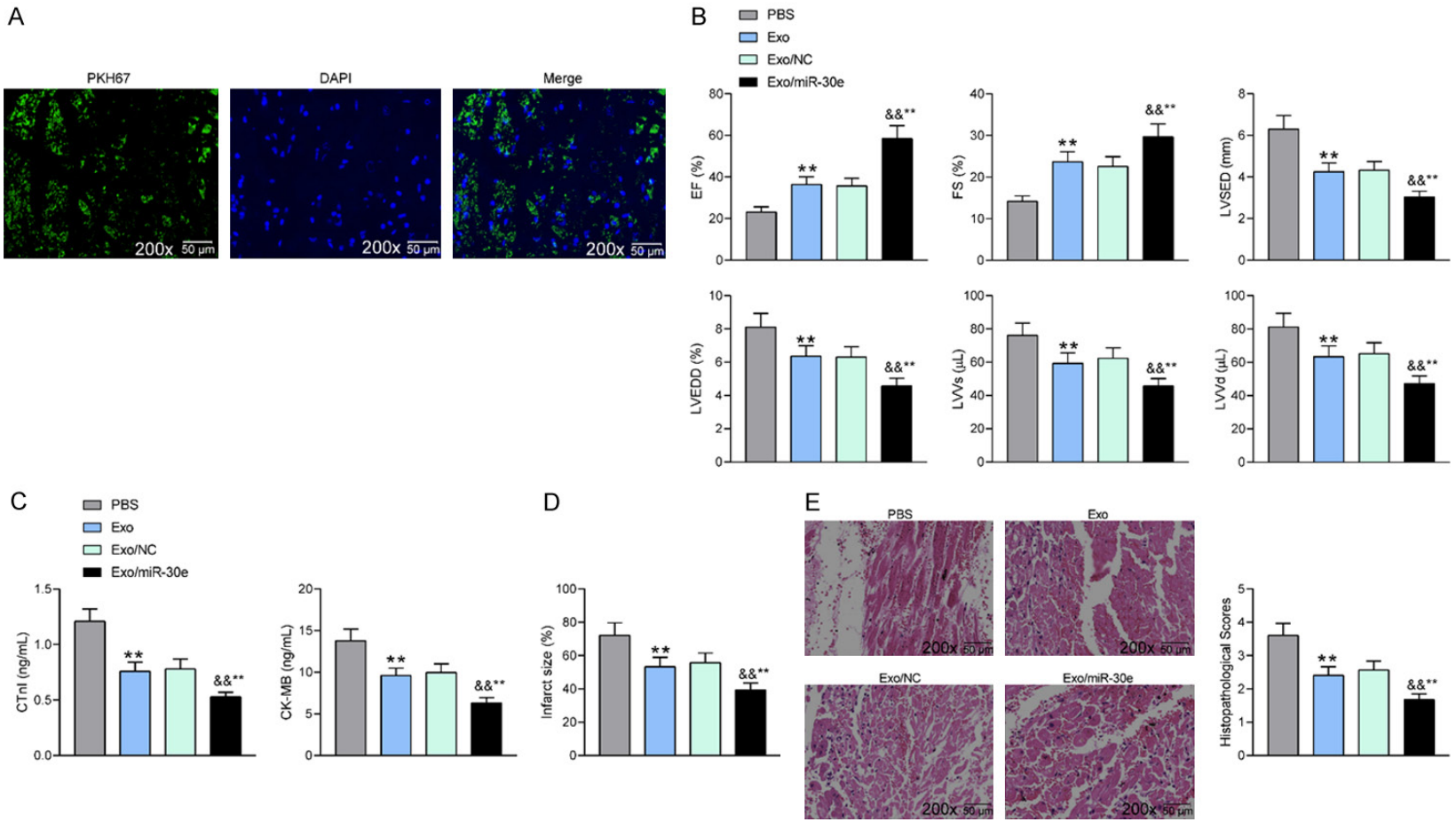

Figure 3. Exo/miR-30e alleviates HF in MI rats. MI rats were injected with Exo derived from BMMSCs transfected with miR-30e mimic or NC or without transfection. (A) Fluorescence detection of PKH67 distribution in rat myocardial tissues; (B) EF, FS, LVEDD, LVESD, LVVs and LVVd values in rats; (C) ELISA for the detection of myocardial injury-related proteins CK-MB and CTnI in the serum of rats; (D) Statistical analysis of infarct size in rat myocardial tissues; (E) HE staining for pathological damage scores in rat myocardial tissues. For (A-E), each group contained 6 rats (one-way ANOVA and Tukey's multiple comparison test). Error bars represent the mean ± SD. $^{**}P < 0.01$ *vs* MI rats injected with PBS; $\&\&P < 0.01$ *vs* MI rats injected with Exo/NC.

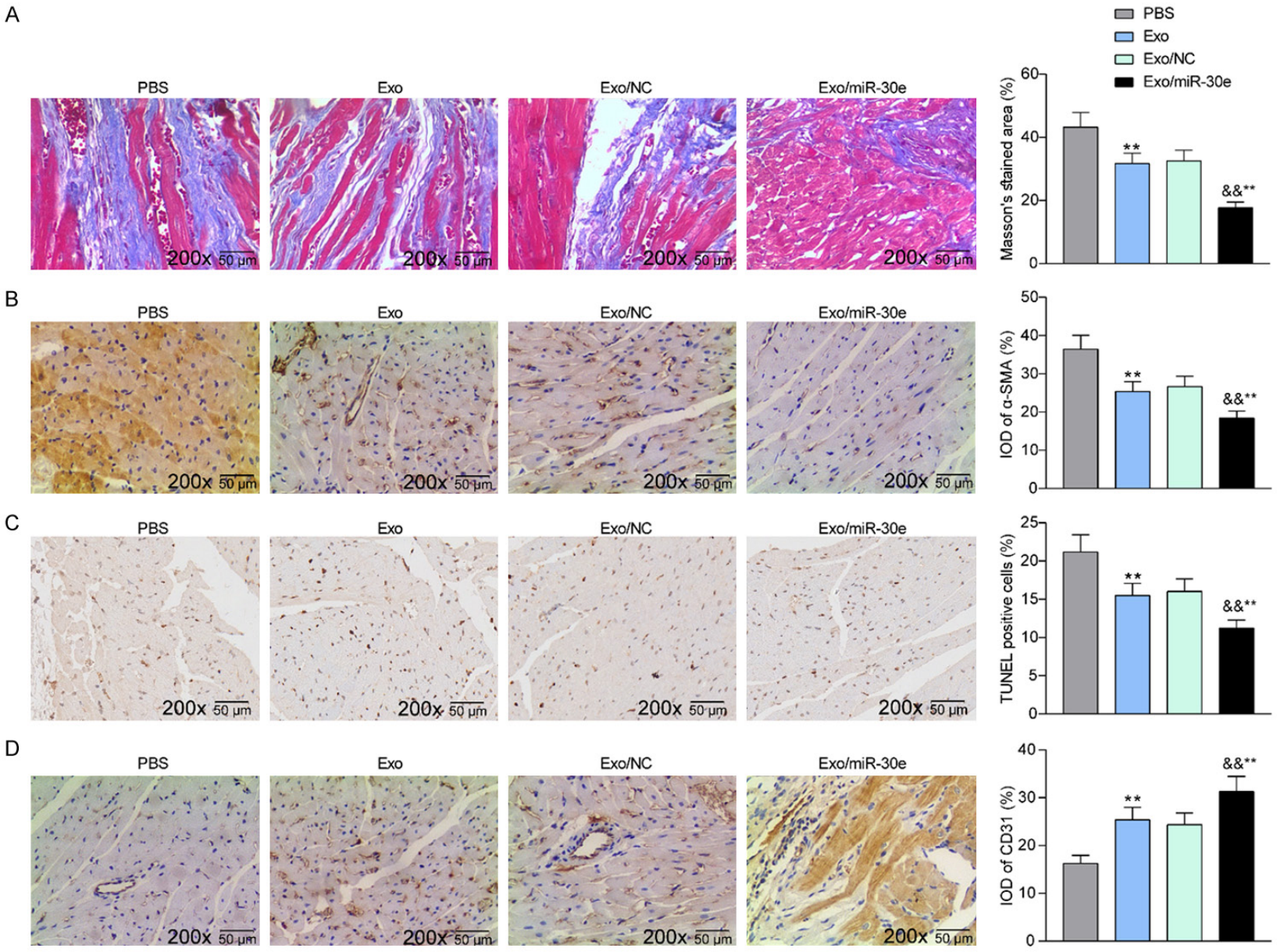
A
PBS
Exo
Exo/NC
Exo/miR-30e
200x 50 μm
Masson's stained area (%)
B
IOD of α-SMA (%)
C
TUNEL positive cells (%)
D
IOD of CD31 (%)
**
&&**

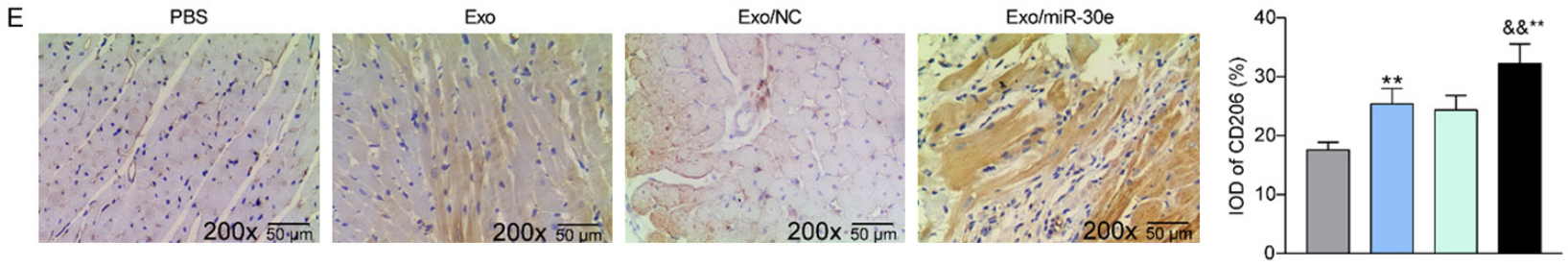

Figure 4. Exo/miR-30e mitigates MI-induced myocardial injury. (A) Masson's staining for the area of collagen deposition in rat myocardial tissue; (B) Immunohistochemical detection of staining intensity of α-SMA in rat myocardial tissues; (C) TUNEL staining for apoptosis in rat myocardial tissues; (D, E) Immunohistochemical detection of the number of positive cells for CD31 (D) and CD206 (E) in myocardial tissue. For (A-E) each group contained 6 rats (one-way ANOVA and Tukey's multiple comparison test). Error bars represent the mean ± SD. $^{**}P < 0.01$ *vs* MI rats injected with PBS; $\&\&P < 0.01$ *vs* MI rats injected with Exo/NC.

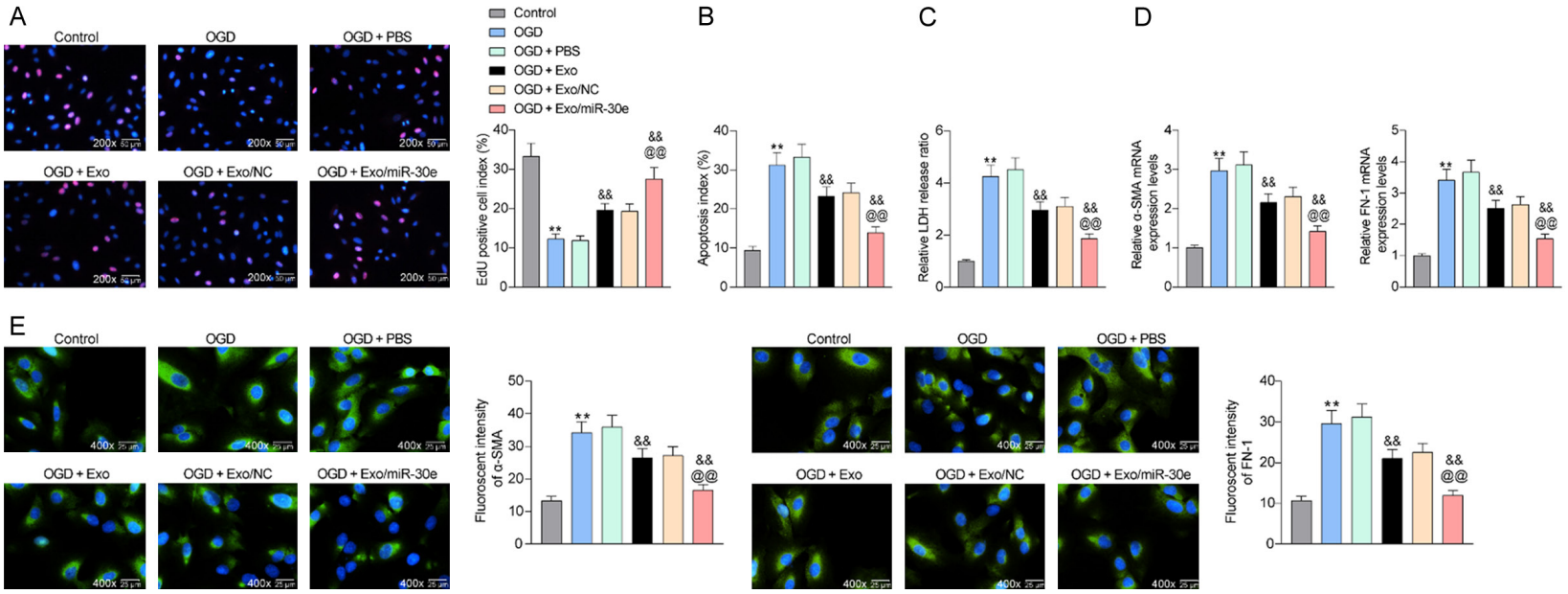

Figure 5. Exo/miR-30e inhibits apoptosis in OGD-treated cardiomyocytes. H9C2 cells exposed to OGD were co-cultured with Exo derived from BMMSCs transfected with miR-30e mimic or NC or without transfection. (A) EdU staining for activity of H9C2 cells; (B) Flow cytometric analysis of apoptosis percentage in H9C2 cells; (C) LDH kits for cytotoxicity caused by OGD treatment; (D, E) RT-qPCR (D) and immunofluorescence detection (E) of α-SMA and FN-1 expression in cells. Error bars represent the mean ± SD. For (A-E) one-way ANOVA and Tukey's multiple comparison test. The results of the experiment were tested in three separate trials. $^{**}P < 0.01$ *vs* H9C2 cells exposed to normoxia; $\&\&P < 0.01$ *vs* H9C2 cells exposed to OGD and treated with PBS; $@@P < 0.01$ *vs* H9C2 cells exposed to OGD and treated with Exo/NC.

flow cytometry (**Figure 5C**). Furthermore, the levels of α-SMA and FN-1 in H9C2 cells were then examined by RT-qPCR after OGD treatment. OGD treatment significantly increased the levels of fibrosis-related factors, but Exo treatment significantly inhibited the fibrosis of H9C2 cells. The increase of Exo-bearing miR-30e further lowered the expression of α-SMA and FN-1 (**Figure 5D**). As expected, immunofluorescence results showed consistent experimental results (**Figure 5E**).

miR-30e negatively regulates LOX1 expression via direct targeting

To expound the downstream mechanism of miR-30e, we first downloaded the gene expression microarray GSE35088 from the GEO database, which contained myocardial tissues from eight MI rats and eight sham-operated rats. The microarray was then screened by setting Log FoldChange > 2 and Adj *p* value < 0.05 as the threshold. We obtained 71 differentially expressed genes (**Figure 6A**, **6B**). The target mRNAs for miR-30e were predicted by StarBase and TargetScan websites, which were cross-screened with genes upregulated in GSE35088. LOX1 was the only one in the intersection (**Figure 6C**). We found a significant increase in LOX1 expression in myocardial tissues of rats after MI surgery, but further treatment with Exo led to a significant decrease in LOX1 expression levels. By contrast, increasing the expression of miR-30e in Exo further inhibited LOX1 expression (**Figure 6D**, **6E**). The same experimental results were seen in OGD-treated H9C2 cells (**Figure 6F**, **6G**). Thus, we examined the binding relationship between miR-30e and LOX1 by dual-luciferase experiments. The luciferase activity was notably downregulated in 293T cells transfected with miR-30e mimic and LOX1-wt (**Figure 6H**, **6I**). Moreover, we performed RIP experiments using anti-Ago2 after transfecting the overexpression plasmids of miR-30e and mimic NC into H9C2 cells. The enrichment levels of miR-30e and LOX1 in the complexes pulled down by the anti-Ago2 antibody were much higher than those of IgG (**Figure 6J**).

LOX1 attenuates the protective effects of BMMSC-Exo on H9C2 cells against injuries induced by OGD

To elucidate the role of LOX1 on myocardial injury, we transfected an overexpression plasmid of LOX1 into H9C2 cells and verified the successful transfection (**Figure 7A**, **7B**). We found that overexpression of LOX1 suppressed H9C2 activity induced by Exo/miR-30e (**Figure 7C**) and increased the proportion of apoptosis in the cells (**Figure 7D**). Moreover, increasing LOX1 expression in H9C2 cells notably boosted the cytotoxicity caused by OGD treatment (**Figure 7E**). Also, overexpression of LOX1 significantly promoted OGD-induced cell fibrosis (**Figure 7F**).

LOX1 promotes HF after MI through activation of the NF-κB p65/Caspase-9 axis

To clarify the downstream mechanism of LOX1, we reviewed the literature and learned that Trichosanthes kirilowii lectin alleviated diabetic nephropathy by inhibiting the LOX1/NF-κB p65/Caspase-9 axis [14]. Therefore, the activity of this signaling was checked in rats. The phosphorylation level of p65 and the expression of caspase-9 were significantly increased after LAD surgery, but further treatment with Exo remarkably inhibited the extent of p65 phosphorylation and the expression of caspase-9, and the effect of Exo/miR-30e was more pronounced than that of Exo (**Figure 8A**). Immunohistochemistry also exhibited the consistent experimental results (**Figure 8B**). Moreover, we further examined the activity of NF-κB p65/Caspase-9 signaling in H9C2 cells and observed that OGD treatment boosted the activity of NF-κB p65/Caspase-9 signaling in cells, but Exo and Exo/miR-30e treatments blocked the NF-κB p65/Caspase-9 signaling activation after OGD exposure. Further overexpression of LOX1 restored the NF-κB p65/Caspase-9 signaling activation in H9C2 cells (**Figure 8C**). Furthermore, immunofluorescence was conducted to detect subcellular localization of phosphorylated NF-κB p65 and noted that OGD treatment accelerated NF-κB p65 nuclear translocation, but Exo treatment notably suppressed the proportion of NF-κB p65 in the nucleus, and further overexpression of LOX1 remarkably increased NF-κB p65 in the nucleus (**Figure 8D**). Thus, to confirm the role of NF-κB p65/Caspase-9 signaling in MI, we treated OGD-exposed cardiomyocytes with the NF-κB p65 inhibitor FW1256. After inhibition of the NF-κB p65 activity, the apoptosis rate of OGD-treated cells decreased significantly (**Figure 8E**), cell activity was significantly increased (**Figure 8F**), and fibrosis levels were

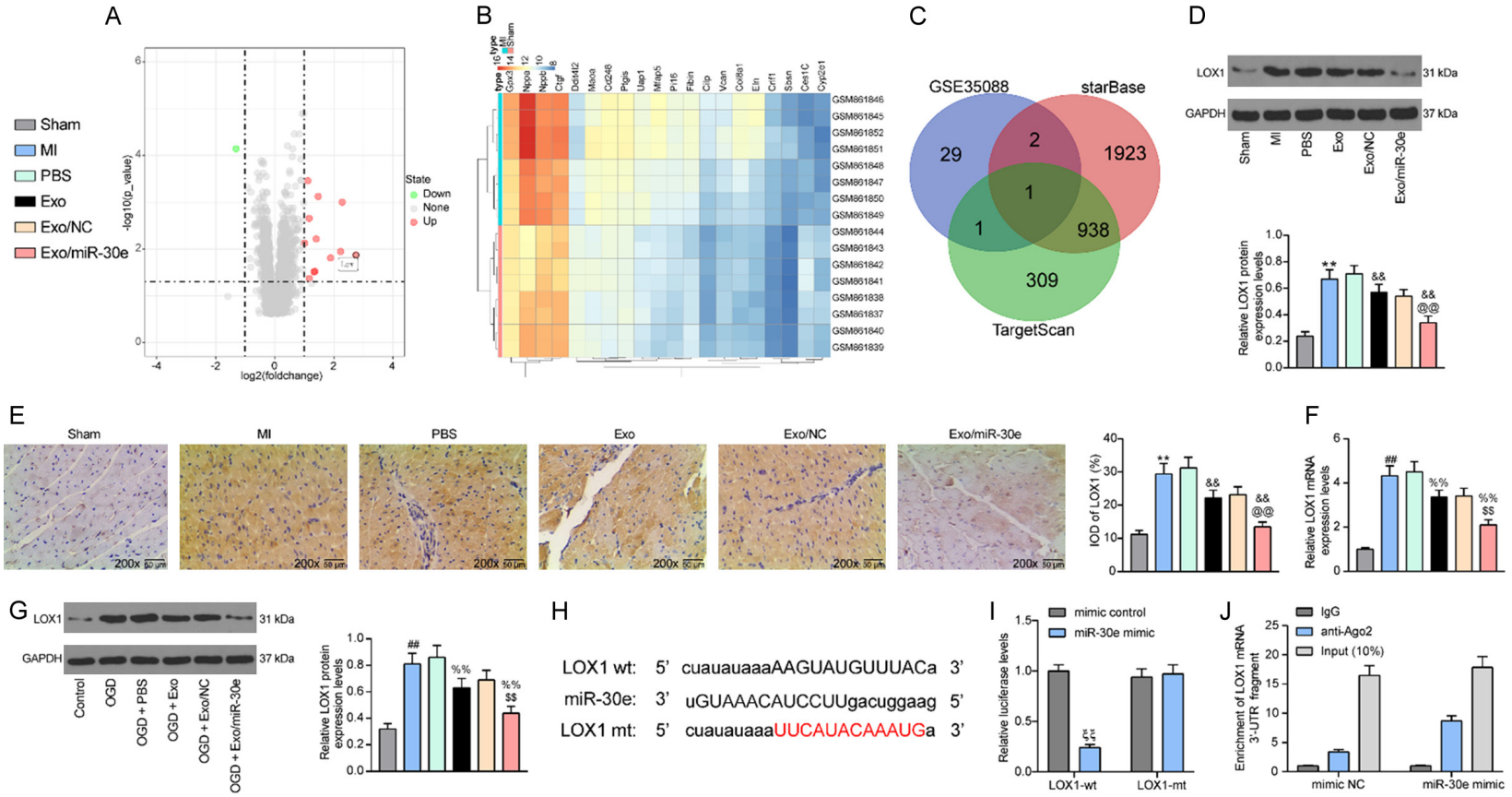

Figure 6. miR-30e negatively regulates LOX1 expression by direct targeting. (A) The volcano map for differentially expression mRNAs in GSE35088 (n = 8); (B) The heatmap for differentially expression mRNAs in GSE35088 (n = 8); (C) The intersection between the prediction of target mRNAs for miR-30e in StarBase (http://starbase.sysu.edu.cn/) and TargetScan (http://www.targetscan.org/vert_72/) websites and genes upregulated in GSE35088; (D, E) Western blot (D) and immunohistochemistry (E) for LOX1 expression in rat myocardial tissues; (F, G) RT-qPCR (F) and western blot detection (G) of LOX1 expression in H9C2 cells; (H) The binding site of miR-30e to the 3'-UTR sequence of LOX1 mRNA; (I, J) Dual-luciferase experiment (I) and RIP experiment validation (J) of the binding relationship between miR-30e and LOX1. For (D and E) each group contained 6 rats (one-way ANOVA and Tukey's multiple comparison test). Error bars represent the mean ± SD. $^{**}P < 0.01$ *vs* sham-operated rats; $\&\&P < 0.01$ *vs* MI rats injected with PBS; $@@P < 0.01$ *vs* MI rats injected with Exo/NC. For (F and G) one-way ANOVA and Tukey's multiple comparison test. The results of the experiment were tested in three separate trials. $\#\#P < 0.01$ *vs* H9C2 cells exposed to normoxia; $\%\%P < 0.01$ *vs* H9C2 cells exposed to OGD and treated with PBS; $\$\$P < 0.01$ *vs* H9C2 cells exposed to OGD and treated with Exo/NC. For (I), two-way ANOVA and Tukey's multiple comparison test. $^{\S\S}P < 0.01$ *vs* mimic control transfection.

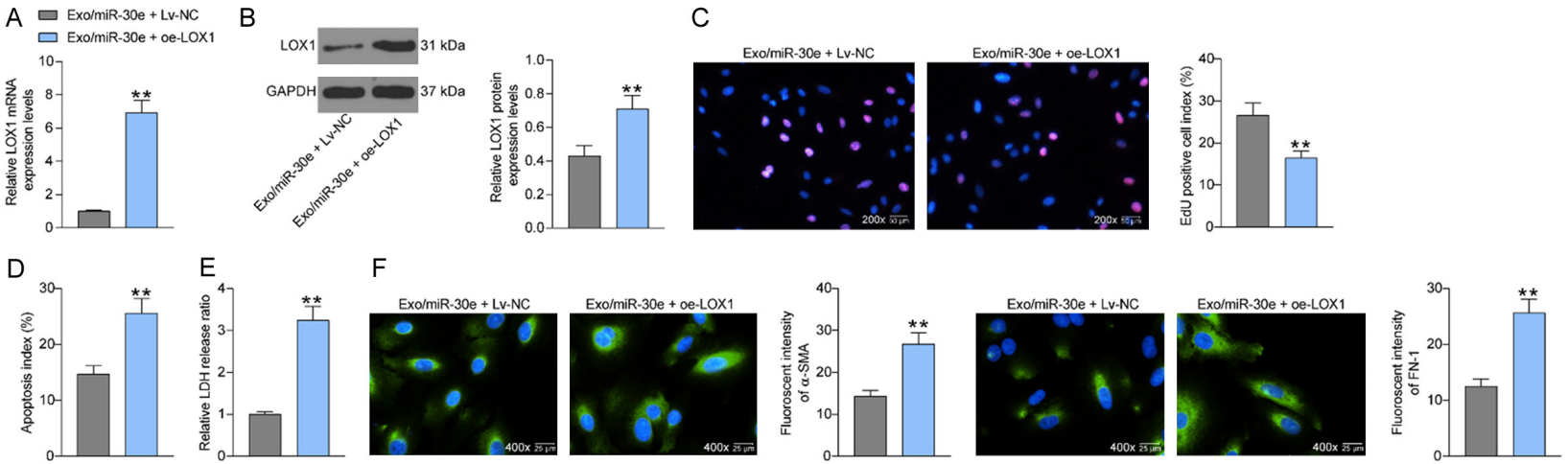

Figure 7. LOX1 overexpression in H9C2 cells attenuates the protective effect of BMMSC-Exo after OGD. H9C2 cells were transfected with LOX1 overexpression, exposed to OGD and co-cultured with Exo derived from BMMSCs transfected with miR-30e mimic or NC. (A, B) RT-qPCR (A) and western blot detection (B) of LOX1 expression in H9C2 cells; (C) EdU staining for activity of H9C2 cells; (D) Flow cytometric analysis of apoptosis percentage in H9C2 cells; (E) LDH kits for cytotoxicity caused by OGD treatment; (F) Immunofluorescence detection of α-SMA and FN-1 expression in cells. Error bars represent the mean ± SD. For (A-F) unpaired *t* test. The results of the experiment were tested in three separate trials. $^{**}P < 0.01$ *vs* H9C2 cells transfected with Lv-NC and co-cultured with Exo derived from BMMSCs transfected with miR-30e mimic.

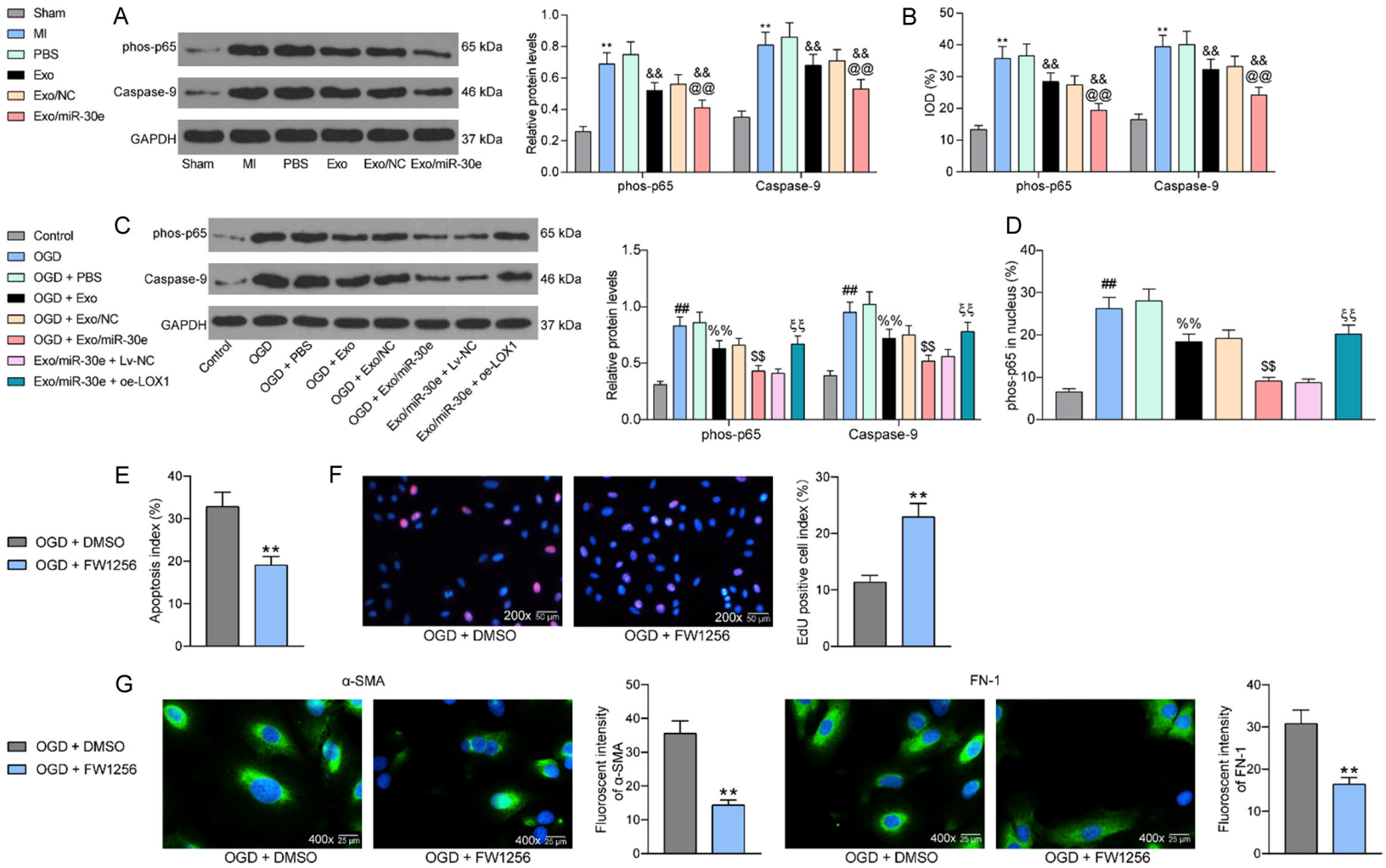

Figure 8. LOX1 promotes HF after MI through activation of the NF-κB p65/Caspase-9 signaling. (A) Western blot detection of p65 phosphorylation and Caspase-9 protein expression in rat myocardial tissues; (B) Staining intensity of phos-p65 and caspase-9 in rat myocardial tissues by immunohistochemical staining; (C) Western blot detection of the activation level of NF-κB p65/Caspase-9 signaling pathway in H9C2 cells; (D) Subcellular localization of phosphorylated NF-κB p65 in H9C2 cells by immunofluorescence detection. NF-κB p65 inhibitor FW1256 or DMSO was applied to OGD-treated cardiomyocytes. (E) Apoptosis level of H9C2 cells by flow cytometry; (F) EdU staining for H9C2 cell activity; (G) Immunofluorescence detection of α-SMA and FN-1 expression in cells. For (A and B) each group contained 6 rats (one-way ANOVA and Tukey's multiple comparison test). Error bars represent the mean ± SD. $^{**}P < 0.01$ *vs* sham-operated rats; &&$P < 0.01$ *vs* MI rats injected with PBS; @@$P < 0.01$ *vs* MI rats injected with Exo/NC. For (C and D) one-way ANOVA and Tukey's multiple comparison test; for (E-G) unpaired *t* test. The results of

the experiment were tested in three separate trials. ##$P < 0.01$ *vs* H9C2 cells exposed to normoxia; %%$P < 0.01$ *vs* H9C2 cells exposed to OGD and treated with PBS; $$$P < 0.01$ *vs* H9C2 cells exposed to OGD and treated with Exo/NC; §§$P < 0.01$ *vs* H9C2 cells transfected with Lv-NC and co-cultured with Exo derived from BMMSCs transfected with miR-30e mimic; ^aa^$P < 0.01$ *vs* H9C2 cells exposed to OGD and treated with DMSO.

significantly reduced (**Figure 8G**). In summary, Exo derived from BMMSC overexpressing miR-30e delivered miR-30e to the myocardial tissues of rats with MI, thereby targeting LOX1 and impairing the activation of NF-κB p65/Caspase-9 signaling to achieve therapeutic effects on HF caused by MI.

Discussion

MSCs have been indicated to be advantageous for improving heart function during the treatment of MI [15]. Meanwhile, Duisters *et al.* established that miR-30 was downregulated in models of pathological hypertrophy and HF [16]. The present study demonstrated that BMMSC-derived Exo exerted cardioprotective effects by transferring miR-30e. By targeting LOX1, miR-30e reduced OGD-induced H9C2 cell apoptosis and cytotoxicity, and improved cardiac function of MI rats. Moreover, LOX1 accentuated injury induced by OGD in H9C2 cells by activating the NF-κB p65/Caspase-9 pathway. Our observations provide fresh insights into the significance of miRNA in the cardio-protection of BMMSC-derived Exo in HF following MI.

After determination of the success modeling of MI rats by assessment of hemodynamics indexes, myocardial injury-related proteins as well as infarct size, we utilized a miRNA array and found that miR-30e was the most downregulated miRNA in myocardial tissues of MI rats. Previously, Ibrahim *et al.* pinpointed that exosomes secreted by human cardiosphere-derived cells are critical for cardio-protection by hampering apoptosis and enhancing proliferation of cardiomyocytes [17]. Moreover, Nakamura *et al.* presented that injection of human adipose tissues-derived MSCs improved cardiac dysfunction in HF induced by pressure overload through releasing Exo [18]. Therefore, we postulated that miR-30e could be transferred by Exo to cardiomyocytes to alleviate HF following MI. Of relevance to this finding, significantly lower expression of miR-30e-5p in extracellular vesicles from plasma was observed in patients with psoriatic arthritis versus those with cutaneous-only psoriasis [19]. To validate our postulation, we transfected miR-30e mimic into BMMSCs for Exo secretion and mouse treatment. As expected, Exo derived from BMMSCs without treatment showed a certain alleviating role in cardiac function, which was further enhanced by miR-30e mimic. Consistently, miR-30e was positively correlated with left ventricular EF in patients with ST-segment elevation MI with primary coronary intervention [20]. In addition, miR-30e suppressed autophagy and apoptosis of cardiomyocytes evoked by Doxorubicin [21]. Overexpression of miR-30e downregulated the apoptosis rate of renal tubular epithelial cells and the expression patterns of vimentin, α-SMA and FN [22]. Our *in vitro* and *in vivo* evidence exhibited that miR-30a reduced the level of fibrosis and the proportion of apoptotic cells in the myocardial tissues of MI rats and H9C2 cells exposed to OGD.

Subsequently, we intersected the prediction of the targeting mRNAs of miR-30e and the upregulated genes in the GSE35088 dataset. LOX1 was identified as the only result. Moreover, we conducted dual-luciferase and RIP assays to verify the binding relationship. The protective role of exosomal miRNAs from MSCs has been underscored in MI previously by targeting different targets, including LOX1 [23-25]. More specifically, exosomal miRNA let-7 from endometrial stem cells derived from menstrual blood alleviated lung fibrosis by targeting LOX1, while enforced expression of LOX1 upregulated the expression patterns of pro-apoptotic proteins [26]. Similarly, our observation from rescue experiments established that LOX1 accentuated the apoptosis, cytotoxicity and fibrosis in H9C2 cells induced by OGD. In oxidative low-density lipoprotein-stimulated endothelial cell injury, the inhibitory effects of miR-320a on apoptosis and LDH release were partially abolished by LOX1 overexpression [27]. The close interaction between LOX1 and the NF-κB p65/Caspase-9 pathway has been highlighted in diabetic nephropathy and oxidative low-density lipoprotein-stimulated endothelial cell injury [14, 28]. Thus, we believed that the NF-κB p65/

Caspase-9 pathway might be one of the possible downstream pathways in exosomal miR-30e/LOX1-mediated function in MI rats and H9C2 cells exposed to OGD. Hyperosmotic stress has been substantiated to activate p65 and NF-κB-mediated Caspase-9 activation in cardiomyocytes [29]. Furthermore, human urine-derived stem cells protected the kidney against injury induced by ischemia/reperfusion in a rat model via exosomal miR-146a-5p by preventing the nuclear translocation of NF-κB p65 [30]. We also noted that the nuclear translocation of NF-κB p65 induced by OGD was halted by BMMSCs-derived Exo, which was potentiated by overexpression of LOX1. Furthermore, the impairment of the NF-κB p65/Caspase-9 pathway using its inhibitor reduced the apoptosis and fibrosis of H9C2 cells.

Conclusion

In this work, we established that BMMSCs-derived Exo were sufficient to alleviate OGD-induced cell injury and LAD-induced MI. Moreover, we revealed that miR-30e drove these effects of BMMSCs-derived Exo. Henceforward, we suggest that delivery of miR-30e to cardiomyocytes via Exo might be a potent mechanism underlying cardio-protection conveyed by BMMSCs-derived Exo. Furthermore, our study suggested that the blocking of the LOX1/NF-κB p65/Caspase-9 axis is a possible downstream of the protective role of miR-30e. Collectively, our findings offer mechanistic insights into the therapeutic potential of Exo through modulation of specific miRNA cargoes.

Acknowledgements

This work was supported by the Beijing Lab for Cardiovascular Precision Medicine, Beijing, China (PXM2020_014226_000017_003771-32_FCG).

Disclosure of conflict of interest

None.

Address correspondence to: Hong Li, Cardiovascular Department, Beijing Anzhen Hospital, Capital Medical University, No. 2, Anzhen Road, Chaoyang District, Beijing 100029, P. R. China. Tel: +86-13311536200; Fax: +86-13311536200; E-mail: Lihong9081@163.com

References

[1] Chen WW, Gao RL, Liu LS, Zhu ML, Wang W, Wang YJ, Wu ZS, Li HJ, Gu DF, Yang YJ, Zheng Z, Jiang LX and Hu SS. China cardiovascular diseases report 2015: a summary. J Geriatr Cardiol 2017; 14: 1-10.

[2] Zhu F, Meng Q, Yu Y, Shao L and Shen Z. Adult cardiomyocyte proliferation: a new insight for myocardial infarction therapy. J Cardiovasc Transl Res 2020; [Epub ahead of print].

[3] Braunwald E. The war against heart failure: the lancet lecture. Lancet 2015; 385: 812-824.

[4] Cahill TJ, Choudhury RP and Riley PR. Heart regeneration and repair after myocardial infarction: translational opportunities for novel therapeutics. Nat Rev Drug Discov 2017; 16: 699-717.

[5] Williams AR and Hare JM. Mesenchymal stem cells: biology, pathophysiology, translational findings, and therapeutic implications for cardiac disease. Circ Res 2011; 109: 923-940.

[6] Shafei AE, Ali MA, Ghanem HG, Shehata AI, Abdelgawad AA, Handal HR, Talaat KA, Ashaal AE and El-Shal AS. Mesenchymal stem cell therapy: a promising cell-based therapy for treatment of myocardial infarction. J Gene Med 2017; 19: e2995.

[7] Miao C, Lei M, Hu W, Han S and Wang Q. A brief review: the therapeutic potential of bone marrow mesenchymal stem cells in myocardial infarction. Stem Cell Res Ther 2017; 8: 242.

[8] Henning RJ. Cardiovascular exosomes and microRNAs in cardiovascular physiology and pathophysiology. J Cardiovasc Transl Res 2021; 14: 195-212.

[9] Wei J, Hollabaugh C, Miller J, Geiger PC and Flynn BC. Molecular cardioprotection and the role of exosomes: the future is not far away. J Cardiothorac Vasc Anesth 2021; 35: 780-785.

[10] Sun T, Dong YH, Du W, Shi CY, Wang K, Tariq MA, Wang JX and Li PF. The role of microRNAs in myocardial infarction: from molecular mechanism to clinical application. Int J Mol Sci 2017; 18: 745.

[11] D'Alessandra Y, Devanna P, Limana F, Straino S, Di Carlo A, Brambilla PG, Rubino M, Carena MC, Spazzafumo L, De Simone M, Micheli B, Biglioli P, Achilli F, Martelli F, Maggiolini S, Marenzi G, Pompilio G and Capogrossi MC. Circulating microRNAs are new and sensitive biomarkers of myocardial infarction. Eur Heart J 2010; 31: 2765-2773.

[12] Marfella R, Di Filippo C, Potenza N, Sardu C, Rizzo MR, Siniscalchi M, Musacchio E, Barbieri M, Mauro C, Mosca N, Solimene F, Mottola MT, Russo A, Rossi F, Paolisso G and D'Amico M. Circulating microRNA changes in heart failure patients treated with cardiac resynchroniza-

tion therapy: responders vs non-responders. Eur J Heart Fail 2013; 15: 1277-1288.
[13] Wang C, Fei Y, Xu C, Zhao Y and Pan Y. Bone marrow mesenchymal stem cells ameliorate neurological deficits and blood-brain barrier dysfunction after intracerebral hemorrhage in spontaneously hypertensive rats. Int J Clin Exp Pathol 2015; 8: 4715-4724.
[14] Lu J, Peng J, Xiang M, He L, Wang D, Xiong G and Li S. Trichosanthes kirilowii lectin alleviates diabetic nephropathy by inhibiting the LOX1/NF-kappaB/caspase-9 signaling pathway. Biosci Rep 2018; 38: BSR20180071.
[15] Jeong H, Yim HW, Park HJ, Cho Y, Hong H, Kim NJ and Oh IH. Mesenchymal stem cell therapy for ischemic heart disease: systematic review and meta-analysis. Int J Stem Cells 2018; 11: 1-12.
[16] Duisters RF, Tijsen AJ, Schroen B, Leenders JJ, Lentink V, van der Made I, Herias V, van Leeuwen RE, Schellings MW, Barenbrug P, Maessen JG, Heymans S, Pinto YM and Creemers EE. miR-133 and miR-30 regulate connective tissue growth factor: implications for a role of microRNAs in myocardial matrix remodeling. Circ Res 2009; 104: 170-178, 176p following 178.
[17] Ibrahim AG, Cheng K and Marban E. Exosomes as critical agents of cardiac regeneration triggered by cell therapy. Stem Cell Reports 2014; 2: 606-619.
[18] Nakamura Y, Kita S, Tanaka Y, Fukuda S, Obata Y, Okita T, Nishida H, Takahashi Y, Kawachi Y, Tsugawa-Shimizu Y, Fujishima Y, Nishizawa H, Takakura Y, Miyagawa S, Sawa Y, Maeda N and Shimomura I. Adiponectin stimulates exosome release to enhance mesenchymal stem-cell-driven therapy of heart failure in mice. Mol Ther 2020; 28: 2203-2219.
[19] Pasquali L, Svedbom A, Srivastava A, Rosen E, Lindqvist U, Stahle M, Pivarcsi A and Sonkoly E. Circulating microRNAs in extracellular vesicles as potential biomarkers for psoriatic arthritis in patients with psoriasis. J Eur Acad Dermatol Venereol 2020; 34: 1248-1256.
[20] Su Q, Ye Z, Sun Y, Yang H and Li L. Relationship between circulating miRNA-30e and no-reflow phenomenon in STEMI patients undergoing primary coronary intervention. Scand J Clin Lab Invest 2018; 78: 318-324.
[21] Lai L, Chen J, Wang N, Zhu G, Duan X and Ling F. MiRNA-30e mediated cardioprotection of ACE2 in rats with Doxorubicin-induced heart failure through inhibiting cardiomyocytes autophagy. Life Sci 2017; 169: 69-75.
[22] Zhao D, Jia J and Shao H. miR-30e targets GLIPR-2 to modulate diabetic nephropathy: in vitro and in vivo experiments. J Mol Endocrinol 2017; 59: 181-190.
[23] He Q, Wang F, Honda T, James J, Li J and Redington A. Loss of miR-144 signaling interrupts extracellular matrix remodeling after myocardial infarction leading to worsened cardiac function. Sci Rep 2018; 8: 16886.
[24] Peng Y, Zhao JL, Peng ZY, Xu WF and Yu GL. Exosomal miR-25-3p from mesenchymal stem cells alleviates myocardial infarction by targeting pro-apoptotic proteins and EZH2. Cell Death Dis 2020; 11: 317.
[25] Qiao L, Hu S, Liu S, Zhang H, Ma H, Huang K, Li Z, Su T, Vandergriff A, Tang J, Allen T, Dinh PU, Cores J, Yin Q, Li Y and Cheng K. microRNA-21-5p dysregulation in exosomes derived from heart failure patients impairs regenerative potential. J Clin Invest 2019; 129: 2237-2250.
[26] Sun L, Zhu M, Feng W, Lin Y, Yin J, Jin J and Wang Y. Exosomal miRNA Let-7 from menstrual blood-derived endometrial stem cells alleviates pulmonary fibrosis through regulating mitochondrial DNA damage. Oxid Med Cell Longev 2019; 2019: 4506303.
[27] Zhang C, Yang H, Li Y, Huo P and Ma P. LNCRNA OIP5-AS1 regulates oxidative low-density lipoprotein-mediated endothelial cell injury via miR-320a/LOX1 axis. Mol Cell Biochem 2020; 467: 15-25.
[28] Zhang Q, Liu J, Liu J, Huang W, Tian L, Quan J, Wang Y and Niu R. oxLDL induces injury and defenestration of human liver sinusoidal endothelial cells via LOX1. J Mol Endocrinol 2014; 53: 281-293.
[29] Eisner V, Quiroga C, Criollo A, Eltit JM, Chiong M, Parra V, Hidalgo K, Toro B, Diaz-Araya G and Lavandero S. Hyperosmotic stress activates p65/RelB NFkappaB in cultured cardiomyocytes with dichotomic actions on caspase activation and cell death. FEBS Lett 2006; 580: 3469-3476.
[30] Li X, Liao J, Su X, Li W, Bi Z, Wang J, Su Q, Huang H, Wei Y, Gao Y, Li J, Liu L and Wang C. Human urine-derived stem cells protect against renal ischemia/reperfusion injury in a rat model via exosomal miR-146a-5p which targets IRAK1. Theranostics 2020; 10: 9561-9578.